



1 **Global dryland aridity changes indicated by atmospheric,**
2 **hydrological, and vegetation observations at meteorological**
3 **stations**

4 Haiyang Shi^{1,6}, Geping Luo^{2,3,4,6}, Olaf Hellwich⁷, Xiufeng He¹, Alishir Kurban^{2,3,4,6}, Philippe De
5 Maeyer^{2,3,5,6} and Tim Van de Voorde^{5,6}

6

7 ¹ School of Earth Sciences and Engineering, Hohai University, Nanjing 211100, China.

8 ² State Key Laboratory of Desert and Oasis Ecology, Xinjiang Institute of Ecology and Geography,
9 Chinese Academy of Sciences, Urumqi, Xinjiang, 830011, China.

10 ³ College of Resources and Environment, University of the Chinese Academy of Sciences, 19 (A) Yuquan
11 Road, Beijing, 100049, China.

12 ⁴ The National Key Laboratory of Ecological Security and Sustainable Development in Arid Region
13 (proposed), Chinese Academy of Sciences, Urumqi, China.

14 ⁵ Department of Geography, Ghent University, Ghent 9000, Belgium.

15 ⁶ Sino-Belgian Joint Laboratory of Geo-Information, Ghent, Belgium.

16 ⁷ Department of Computer Vision & Remote Sensing, Technische Universität Berlin, 10587 Berlin,
17 Germany.

18

19 **Correspondence to:** Geping Luo (luogp@ms.xjb.ac.cn) and Olaf Hellwich (olaf.hellwich@tu-berlin.de)

20

21

22



23 **Abstract**

24 In the context of global warming, an increase in atmospheric aridity and global dryland expansion were
25 expected under the future climate in previous studies. However, it conflicts with observed greening
26 over drylands and the insignificant increase in hydrological and ecological aridity from the
27 ecohydrology perspective. Combining climatic, hydrological, and vegetation data, this study evaluated
28 global dryland aridity changes at meteorological sites from 2003 to 2019. A decoupling between
29 atmospheric, hydrological, and vegetation aridity was found. Atmospheric aridity represented by the
30 vapour pressure deficit (VPD) increased, hydrological aridity indicated by machine learning-based
31 precipitation minus evapotranspiration (P-ET) data did not change significantly, and ecological aridity
32 represented by leaf area index (LAI) decreased. P-ET showed non-significant changes in most of the
33 dominant combinations of VPD, LAI, and P-ET. This study highlights the added values of using station
34 scale data to assess dryland change as a complement to the results based on coarse resolution reanalysis
35 data and land surface models.

36 **1 Introduction**

37 Drylands are defined as regions with a dry climate, limited water, and scarce vegetation (Berg and
38 McColl, 2021). In the context of global warming, due to potential higher atmospheric water demand,
39 the global dryland is expected to expand. It will severely affect the relevant ecosystem functions and
40 livelihoods in drylands (Reynolds et al., 2007; Yao et al., 2020; Prāvālie, 2016). To date, there are still
41 major limitations in the consensual knowledge and consistent understanding of global dryland aridity
42 changes, such as wet-dry changes, the location, magnitude, and persistence of the potential dryland
43 expansion and associated mechanisms (Berg and McColl, 2021; Lian et al., 2021; Huang et al., 2016,
44 2017; Grünzweig et al., 2022; Pan et al., 2021). Such knowledge gaps have substantially limited the
45 effective climate adaptation and related strategy development to realize the Sustainable Development
46 Goals in drylands, especially in the global south (Li et al., 2021; Fu et al., 2021; Yao et al., 2021;
47 Ramón Vallejo et al., 2012).

48

49 The difficulty of the current investigation on dryland change lies in its multifaceted nature including
50 the diverse characteristics of climate, hydrology, and ecosystems. The indicators and methods used to



51 assess changes in drylands are thus diverse and previous studies have obtained different findings (Lian
52 et al., 2021) on dryland change. Typically, the arid index (AI), calculated as the multi-year average
53 precipitation (P) divided by potential evaporation (PET), was commonly used to measure atmospheric
54 aridity in long-term global dryland change measuring studies (Huang et al., 2017, 2016). It used only
55 atmospheric inputs, focused only on atmospheric aridity, and did not take into account the effects of
56 ecohydrological aridity and the influence of land surface processes (Berg and McColl, 2021). AI-based
57 studies have found global dryland expansions in the past and future (Huang et al., 2017, 2016) in the
58 global warming context. However, such AI-based finding appears to be contrary to the global greening
59 of dryland vegetation based on satellite remote sensing observations (Fensholt et al., 2012; Poulter et
60 al., 2014; Lian et al., 2021; Hickler et al., 2005; Zhu et al., 2016). This illustrated the necessity of
61 incorporating changes in surface properties such as vegetation in addition to atmospheric indicators.
62 Therefore, from an ecohydrological perspective, recent studies have employed various ecohydrological
63 indicators and land-surface-property changes such as soil moisture, vegetation greenness,
64 evapotranspiration (ET), P-ET (i.e., P minus ET as surface water availability), and runoff to assess the
65 dryland change (Berg and McColl, 2021; Lian et al., 2021; Denissen et al., 2022; Yang et al., 2018;
66 Milly and Dunne, 2016; He et al., 2019). Such recent studies have shown that the dryland changes
67 indicated by land surface changes and ecohydrological indicators did not confirm the ‘expansion of
68 drylands’ finding in previous atmospheric-indicator-based studies (Huang et al., 2016, 2017; Feng and
69 Fu, 2013). In terms of the mechanism explanation, these studies claimed that atmospheric drying and
70 vegetation greening may occur simultaneously, and elevated vapour pressure deficit (VPD) does not
71 fully propagate to surface changes to exacerbate decreases in soil moisture and runoff. Under elevated
72 atmospheric CO₂, plant stomata may close and reduce transpiration and ET, and improve water use
73 efficiency (WUE) (Lian et al., 2021; Berg and McColl, 2021; Roderick et al., 2015), which may
74 compensate for the negative effects of elevated VPD on vegetation growth. This mechanism was not
75 accounted for the physically based estimates of PET (e.g., the Penman-Monteith equation) and thus AI-
76 based findings may have overestimated the aridity and contained considerable uncertainty.
77
78 However, the data used in most of the above-mentioned approaches have large uncertainties, such as
79 coarse transpiration/ soil moisture data (0.5° × 0.5° resolution) from long-term climate and land surface



80 model simulations (Berg and McColl, 2021) and coarse soil moisture/ ET data ($0.25^\circ \times 0.25^\circ$
81 resolution) from the Global Land Evaporation Amsterdam Model (GLEAM) or the global land data
82 assimilation system (GLDAS), which are not necessarily applicable to the assessment of dryland
83 expansion at fine scales. In addition, it is difficult to validate the findings in such coarse-resolution
84 studies with ground observations. It is thus essential to make better use of station-scale data, which
85 may have the potential in measuring dryland change at a finer scale, be better combined with ground
86 observations, and provide more effective climate change adaptation suggestions for local communities.
87
88 Therefore, aimed at reducing scale-related uncertainty and obtaining a comprehensive finding of
89 multifaceted characteristics, this study investigated dryland change at the meteorological station scale
90 using the combinations of atmospheric, hydrological, and vegetation condition observations including
91 VPD, P-ET, and leaf area index (LAI). VPD and P are from meteorological observations, LAI is from
92 MODIS imagery. ET is estimated by a Random Forest (RF) model trained from dryland flux stations in
93 FLUXNET2015, and the data-driven methods can avoid uncertainties caused by physically based ET
94 models. At the station scale, this study provides new insights into global dryland aridity change using
95 multifaceted data with a higher proportion of observations.

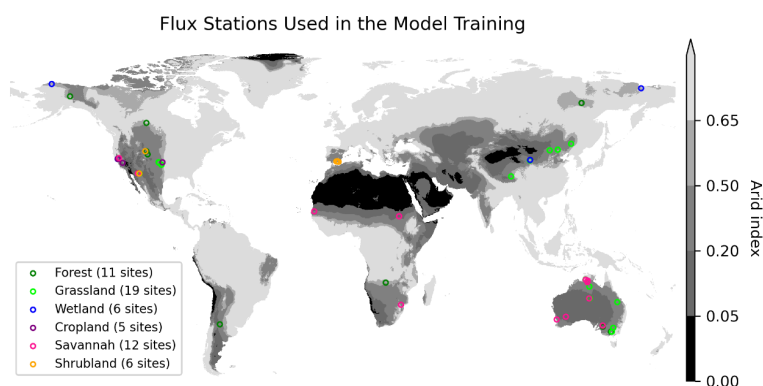
96

97 **2 Methodology**

98 We produced ET data for global dryland meteorological stations by applying an ET machine learning
99 model obtained from FLUXNET2015's dryland flux station ($AI < 0.65$) data trained using RF to global
100 dryland ($AI < 0.65$) meteorological stations. We selected daily ET observations (i.e., latent heat
101 observations) from the FLUXNET2015 dataset for stations in drylands as the target variable. The
102 selected predictor variables include downward shortwave radiation (RSDN), air temperature (T_a), daily
103 variance (half-hourly daily maximum temperature minus daily minimum temperature, T_{Arange}), VPD,
104 wind speed (WS), and LAI from remote sensing (Table 1). Finally, the parameter-optimized RF model
105 was applied to the stations in the drylands of the global meteorological stations in the Global Surface
106 Summary of the Day (GSOD) dataset. In this way, daily-scale ET time series data were predicted for
107 each meteorological station. For each station, when the number of predicted daily ET records for a
108 given year exceeded 100, the annual ET mean was calculated using the arithmetic mean of the daily ET



109 values. Given the absence of data such as LAI during winter snowpack at a small number of arid zone
 110 stations, this approach allows for an effective dense sampling of growing season days to represent
 111 annual ET and distinguish between high and low annual ET values across years. In the subsequent
 112 formal dryland change analysis, cropland meteorological stations were removed due to potential
 113 considerable irrigation influence.
 114



115
 116 Figure 1 The used 59 flux sites in drylands (AI < 0.65) in FLUXNET2015 in the RF model
 117 construction. AI level classification: hyperarid (0 < AI < 0.05), arid (0.05 < AI < 0.2), semiarid (0.2
 118 < AI < 0.5), dry subhumid (0.5 < AI < 0.65).
 119

120 Table 1. Description of the predictors used in the RF model to estimate ET at meteorological stations.

Predictor	Source	Description
LAI	MCD15A3H dataset derived from MODIS data	The 4-daily LAI was linearly interpolated to the daily scale. It was extracted based on Google Earth Engine (GEE) at a scale of 500 m (i.e., cutouts of the 500 × 500 m pixels centered on each station).
RSDN	from the BESS(Ryu et al., 2018) dataset derived from MODIS imagery	It is of 5.5 km spatial resolution. It was extracted based on GEE at a scale of 500 m
WS	In-situ observation	



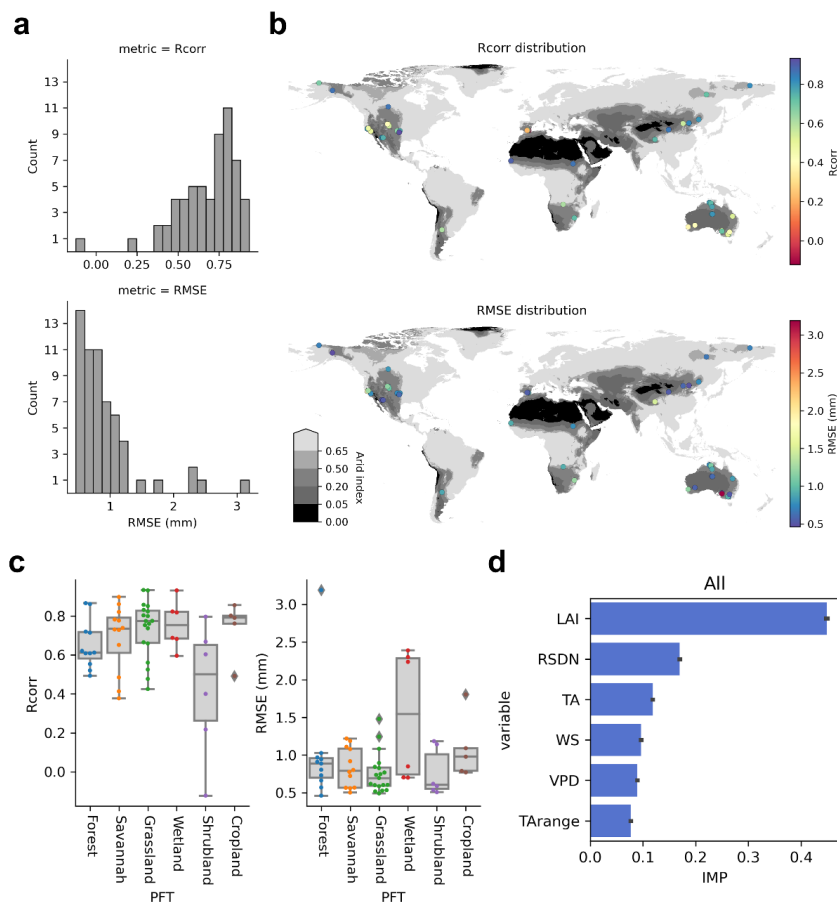
TA	In-situ observation	
TARange	In-situ observation	Daily TARange is derived from the half-hourly maximum temperature and minimum temperature data of FLUXNET2015.
VPD	In-situ observation	VPD is calculated from TAm _{ax} , TAm _{in} , and dew point temperature (Tdew) (Howell and Dusek, 1995).

121

122 **3 Results**

123 **3.1 ET estimation evaluation**

124 We evaluated the performance of the RF model at each flux site using leave-one-site-out cross-
125 validation, and most sites showed high accuracy (Fig. 2) in both Pearson's correlation coefficients
126 (R_{corr}) of observed and predicted daily ET values and RMSE. It indicated the feasibility of accurate
127 daily ET simulations at most dryland flux sites. And among the predictors, LAI had the highest feature
128 importance (Fig. 2d), followed by RSDN, TA, WS, VPD, and TARange. This demonstrated the
129 importance of surface vegetation conditions in ET simulations at dryland sites.



130

131 Figure 2 The model performance and feature importance in the leave-one-site-out cross-validation.

132 (a) Rcorr and RMSE values of 59 sites. (b) Spatial distribution of Rcorr and RMSE records. (c)

133 Rcorr and RMSE of various PFTs. (d) Feature importance (IMP) ranking.

134

135 3.2 Climatic, hydrological, and vegetation changes over drylands

136 The pattern of change in each climate and vegetation variable between the periods 2003-2010 and

137 2011-2019 showed considerable variations (Fig. 3). The number of sites with significant increases in

138 TA, LAI, and VPD was considerably greater than the number of sites with significant decreases. The

139 number of sites with significant increases in P, ET, and P-ET was also greater than the number of sites

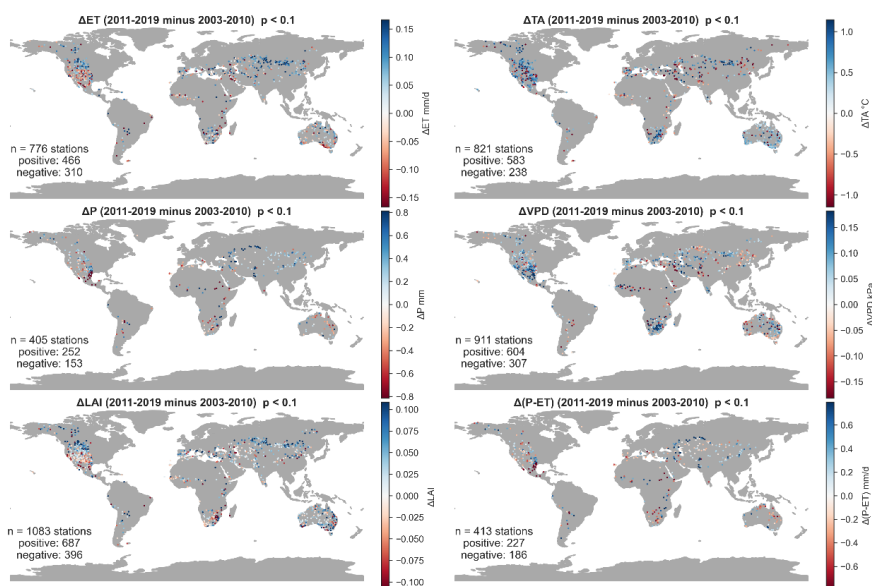
140 with significant decreases. The ratio of the numbers of sites with increases and decreases in P-ET is the

141 lowest. This shows the spatial variability of the trends indicated by the different indicators: the increase



142 in TA and VPD in the context of global warming is widespread and their spatial pattern similarity is
 143 also high. The increasing trend in LAI is also dominant. The spatial pattern of ET changes is highly
 144 similar to that of LAI. Both ET and LAI show significant regional increases in the high latitudes of
 145 North America, and central Eurasia, and decreases in the middle and low latitudes of North America.
 146 The spatial pattern of changes in P-ET is more similar to that of P, but the increase in P is not
 147 completely propagated to P-ET and may be partially offset by the trend in ET.

148



149

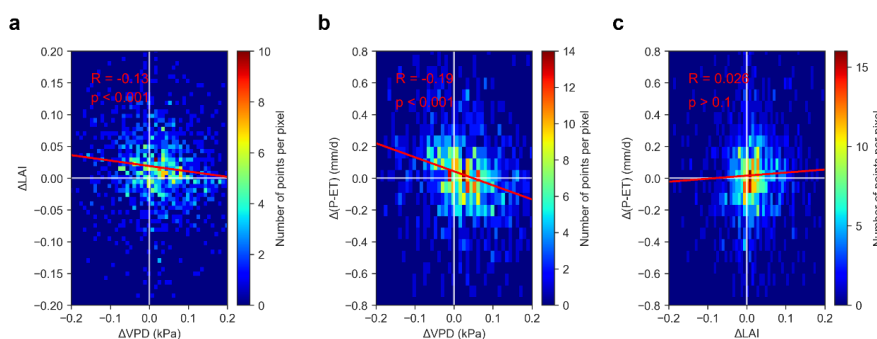
150 Figure 3 Significant changes ($p < 0.1$) in ET, TA, P, VPD, LAI, and P-ET for dryland meteorological
 151 sites (from 2003-2010 to 2011-2019).

152

153 We compared the relationship between ΔVPD , which represents changes in atmospheric aridity, $\Delta P-ET$,
 154 which represents changes in hydrological aridity, and ΔLAI , which represents changes in vegetation
 155 growth. ΔVPD showed a negative correlation with $\Delta P-ET$ ($R = -0.19, p < 0.001$), indicating that
 156 elevated VPD in drylands did lead to a decrease in surface water availability. However, the negative
 157 correlation between ΔVPD and ΔLAI was not strong ($R = -0.13, p < 0.001$), indicating that
 158 atmospheric drying was not a dominant determinant of vegetation greening or browning. The positive
 159 correlation between $\Delta P-ET$ and ΔLAI was not significant ($p > 0.1$), indicating a decoupling between
 160 the greening of dryland vegetation and changes in surface water availability.



161



162

163 Figure 4 Relations of (a) $\Delta\text{LAI}-\Delta\text{VPD}$, (b) $\Delta(\text{P-ET})-\Delta\text{VPD}$, and (c) $\Delta(\text{P-ET})-\Delta\text{LAI}$ at dryland
164 meteorological sites (from 2003-2010 to 2011-2019).

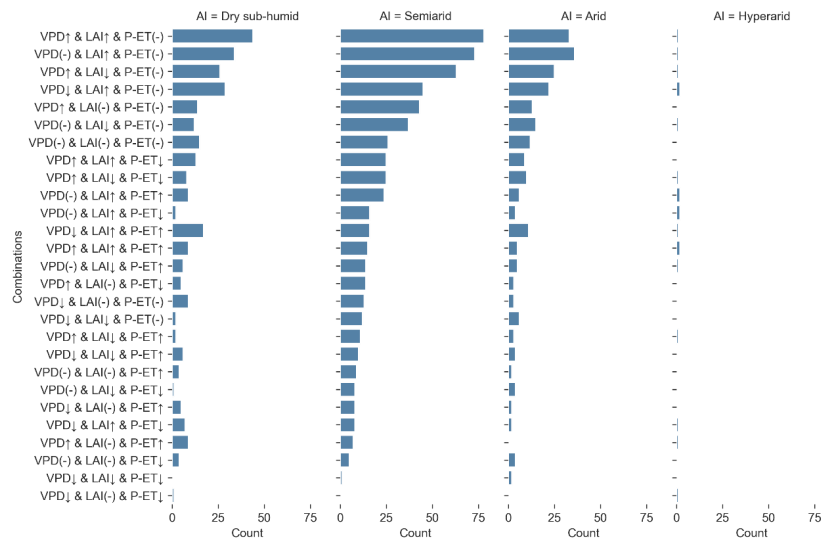
165

166 3.3 Combined atmospheric, hydrological, and vegetation perspectives

167 We also analyzed the combinations of VPD, LAI, and P-ET changes, and the distribution patterns of
168 the different combinations across the globe represented different mechanisms of dryland changes (Fig.
169 5). In the Dry subhumid, Semiarid and Arid regions, three of the top four combinations exhibited
170 significant increases in LAI, while VPD exhibited increases, no significant change, increases, and
171 decreases, respectively. In the top four combinations, the combination with an increase in VPD
172 accompanied by LAI decrease only ranked third or fourth. This suggests that the effect of vegetation
173 browning caused by increasing VPD may not be dominant and that the increasing atmospheric water
174 demand did not considerably decrease vegetation growth. In the Dry subhumid region, compared to the
175 Semiarid and Arid regions, the combinations of 'VPD \downarrow & LAI \uparrow & P-ET (-)' and 'VPD \downarrow & LAI \uparrow & P-
176 ET \uparrow ' combinations ranked higher. It indicates that in the Dry subhumid region, the possibility of the
177 combination of VPD decrease accompanied by LAI increase is higher. In the Arid region, the
178 combination of 'VPD \uparrow & LAI \uparrow & P-ET (-)' dropped from the first to the second in the ranking
179 compared to the Dry sub-humid and Semiarid regions, indicating that when AI is lower, the mechanism
180 represented by the combination of the simultaneous increase in VPD and LAI are less likely to occur.
181 Surprisingly, of the seven combinations of VPD, LAI, and P-ET in the top ranking, P-ET showed no
182 significant change. This suggests a smaller contribution from changes in surface water availability in
183 explaining the variation of combinations of mechanisms for dryland change, although the changes in P-



184 ET and VPD in the lower-ranked combinations showed opposite trends. The surface water represented
185 aridity increase obtained in this study is smaller than that indicated by soil moisture and runoff reported
186 previously (Lian et al., 2021).



187

188 Figure 5 Combinations of VPD, LAI, and P-ET changes across various AI areas from 2003-2010 to
189 2011-2019. The symbol '↑' represents a significant increase ($p < 0.1$) of VPD, LAI, or P-ET. The
190 symbol '↓' represents a significant decrease ($p < 0.1$) and '(-)' represents insignificant changes.

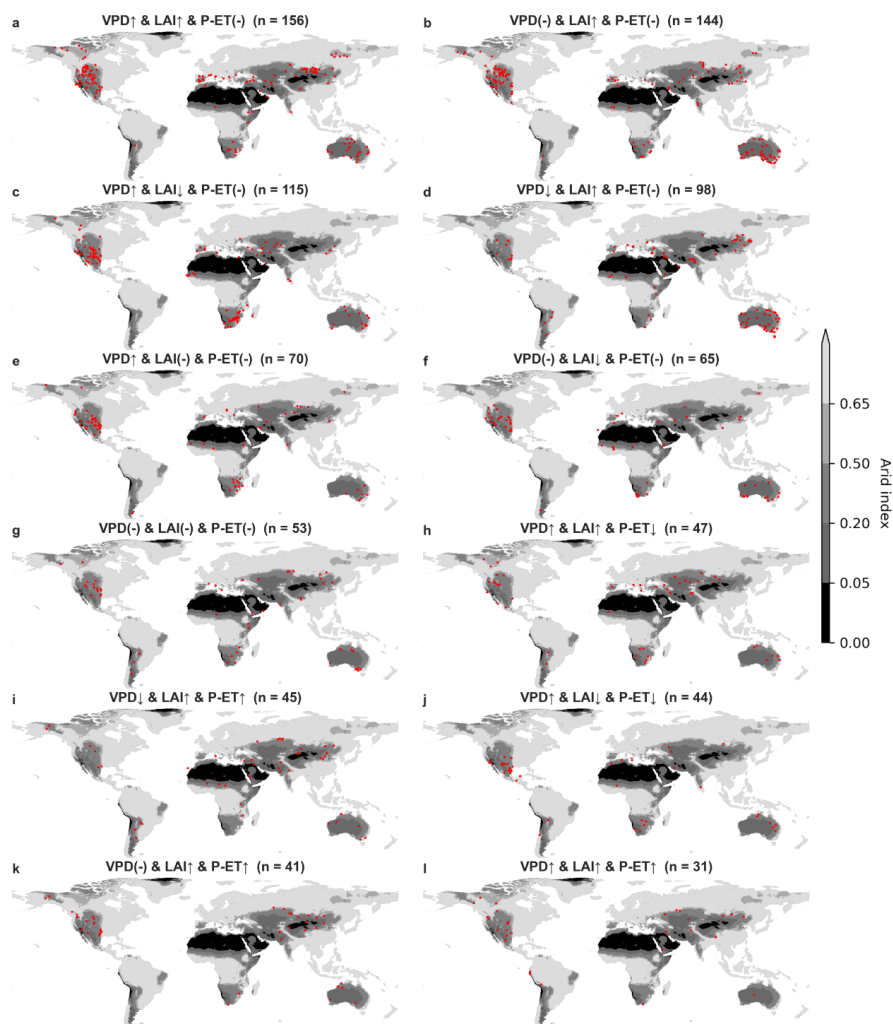
191

192 The distribution of these combinations is also highly heterogeneous spatially, indicating the high
193 regional heterogeneity in global dryland change (Feng et al., 2022; Lian et al., 2021). Given this study
194 is at the station scale, the impacts of heterogeneous underlying surface conditions can be higher.

195 Combinations with non-significant changes in P-ET are widely distributed globally (Fig. 6a,b,c,d,e,f,g),
196 including in the western part of North America, Australia, and southern Europe, where there are more
197 dense stations. Although the combinations of VPD and LAI changes appear to be spatially variable,
198 some regional patterns were still found. For example, 'VPD↑ & LAI↑ & P-ET (-)' is the dominant
199 combination in Mongolian grasslands (Fig. 6a). The increase in LAI due to increased P-ET was also
200 observed in northwest China and northern Central Asia (Fig. 6i, 6k), suggesting that the recent trend of
201 wetting and greening in this region is more likely to be caused by increased surface water availability
202 (Shi et al., 2007). The results of previous coarse regional patterns of dryland change may not



203 necessarily be applicable to the station scale, which needs more station-scale evaluation and
204 validations.
205



206
207 Figure 6 Locations of combinations of VPD, LAI, and P-ET changes from 2003-2010 to 2011-2019.
208 The symbol '↑' represents a significant increase ($p < 0.1$) of VPD, LAI, or P-ET. The symbol '↓'
209 represents a significant decrease ($p < 0.1$) and '(-)' represents insignificant changes.
210



211 **4. Discussions**

212 **4.1 Implications and Perspective**

213 This study investigated the characteristics of dryland change at global dryland meteorological stations
214 using a combination of atmospheric, hydrological, and vegetation indicators. A decoupling between
215 atmospheric, hydrological, and ecological aridity was found in this study, specifically, atmospheric
216 aridity represented by VPD increased, hydrological aridity indicated by P-ET did not change
217 significantly, and ecological aridity represented by LAI decreased. It is consistent with the decoupling
218 found in previous studies based on reanalysis data and coarse-resolution land surface model
219 simulations (Lian et al., 2021) which considered the impacts of elevated CO₂ concentration. This study
220 also found that P-ET showed non-significant changes in most of the dominant combinations of VPD,
221 LAI, and P-ET. This is slightly different from the reported weak aridity hydrological increase in
222 previous studies based on soil moisture and runoff data (Lian et al., 2021), although the year span from
223 2003 to 2019 in the present study was smaller than these studies (usually more than 50 years).

224
225 The value of this study is revisiting the dryland change issue at the station scale. The key to this is the
226 use of a machine learning approach to estimate daily-scale ET data from meteorological stations and to
227 combine the measured P and thus calculate P-ET. Machine learning-based ET simulations (Jung et al.,
228 2010, 2019) may effectively avoid the setting of various hypothetical mechanisms in physics-based ET
229 models (Martens et al., 2017; Zhang et al., 2010; Mu et al., 2011), mine the relationship between
230 dryland ET and various environmental factors such as climate and vegetation from measured data, and
231 achieve a high estimation accuracy. Therefore, the estimation of P-ET at the station scale effectively
232 measured the status of surface water change since soil moisture and runoff data are difficult to obtain at
233 the meteorological station scale. Station-scale studies of dryland change may be a new direction for the
234 future, given the limitation in the coarse resolution of current reanalysis data, land surface models, etc.,
235 and the difficulty of validating their results in the field via ground in situ data. Combined use of
236 climate, hydrological, and vegetation condition variables at the station scale may have the potential to
237 provide an interface for dryland change studies to be more connected to ground observations and
238 associated field experiments. The current satellite remote sensing data still cannot fully capture the
239 physiological and hydraulic characteristics (Zeng et al., 2022) of dryland plants in the context of



240 climate change and extreme weather conditions. It illustrates that station-scale studies will be further
241 important in the future.

242

243 **4.2 Limitations and Uncertainties**

244 **4.2.1 Uncertainties in the ET Estimation**

245 In the past, data for P-ET have rarely been produced at the meteorological station scale, while most in
246 the coarse-resolution grid scale (Jung et al., 2019; Martens et al., 2017; Zhang et al., 2010), and this
247 study combined machine-learning-based estimates of daily ET with actual measurements of P to
248 produce P-ET data for dryland meteorological stations. ET simulations exhibit high accuracy at most
249 stations, but accuracy is limited at a few stations, possibly due to the inefficiency of the selected
250 predictor variables in the explanation of the site-specific ET variations (Shi et al., 2022a). In future
251 studies, it can be effective to incorporate station-specific plant hydraulic characteristics as well as
252 vegetation-trait-related predictor variables (Anderegg, 2015; Anderegg et al., 2018; Shi et al., 2022b;
253 Zhao et al., 2022). In addition, combining data-driven machine learning methods with physical process-
254 based ET estimation models would be promising (Zhao et al., 2019), with the potential to further
255 improve ET simulation accuracy. In addition, it may be beneficial to combine transpiration
256 observations such as SAPFLUXNET (Poyatos et al., 2021) to provide estimates of transpiration.
257 Compared to ET, transpiration can be more precisely correlated to plant physiological and hydraulic
258 characteristics, thus providing more detailed mechanism interpretations in dryland aridity change.

259

260 **4.2.2 Spatial and temporal representativeness of meteorological stations on dryland change**

261 Although meteorological stations can provide more accurate climate, hydrology, and vegetation data at
262 fine scales to support studies associated with dryland change, they may still have limitations in spatial
263 and temporal representativeness. First, the temporal representativeness of meteorological stations is
264 highly variable across different regions of the globe. Inconsistencies in the length of station observation
265 records, etc., may lead to unbalance when comparing between regions. Second, meteorological stations
266 are sparsely located in hyperarid areas, and the representativeness of hyperarid regions can be low. In
267 other dryland types (i.e., Dry subhumid, Semiarid, and Arid), the representativeness of meteorological
268 stations may also be affected by other factors such as human activities. In this study, it was considered



269 that irrigation of dryland cropland could greatly affect the assessment of P-ET and VPD, and therefore
270 stations in croplands were removed. However, other disturbances from human activities may still exist,
271 such as possible grazing (Huang et al., 2018) within the 500 m surrounding extent of the station.

272

273 In contrast, climate adaptation management in surrounding regions of local meteorological stations
274 may not require much attention to the lack of spatial and temporal representativeness. The combined
275 use of station-scale VPD, LAI, and P-ET data would be valuable for the development of associated
276 adaptation policies in local agriculture management and ecological conservation.

277 **5. Conclusion**

278 Combining climatic, hydrological, and vegetation data, this study assesses global dryland change at
279 meteorological sites from 2003 to 2019. A decoupling between atmospheric, hydrological, and
280 ecological aridity was found in this study, specifically, atmospheric aridity represented by VPD
281 increased, hydrological aridity indicated by machine learning-based P-ET data did not change
282 significantly, and ecological aridity represented by LAI decreased. P-ET showed non-significant
283 changes in most of the dominant combinations of VPD, LAI, and P-ET.

284



285 **Acknowledgment**

286 We would like to thank Prof. Pierre Gentine for his insightful suggestions on ET modeling.

287 **Financial support**

288 This research was supported by the Tianshan Talent Cultivation (Grant No. 2022TSYCLJ0001), the
289 Key projects of the Natural Science Foundation of Xinjiang Autonomous Region (Grant No.
290 2022D01D01), the Strategic Priority Research Program of the Chinese Academy of Sciences (Grant
291 No. XDA20060302), and High-End Foreign Experts Project.

292 **Author Contributions**

293 HS and GL initiated this research and were responsible for the integrity of the work as a whole. HS
294 performed formal analysis and calculations and drafted the manuscript. HS was responsible for the data
295 collection and analysis. GL, PDM, TVdV, OH, XH and AK contributed resources and financial support.

296 **Competing interests**

297 The authors declare that they have no conflict of interest.

298 **Code availability**

299 The codes that were used for all analyses are available from the first author (haiyang.shi@hhu.edu.cn).

300 **Data availability**

301 The data used in this study are available from the first author (haiyang.shi@hhu.edu.cn).

302

303



304 **References**

- 305 Anderegg, W. R.: Spatial and temporal variation in plant hydraulic traits and their relevance for
306 climate change impacts on vegetation, *New Phytologist*, 205, 1008–1014, 2015.
- 307 Anderegg, W. R., Konings, A. G., Trugman, A. T., Yu, K., Bowling, D. R., Gabbitas, R., Karp, D.
308 S., Pacala, S., Sperry, J. S., and Sulman, B. N.: Hydraulic diversity of forests regulates ecosystem
309 resilience during drought, *Nature*, 561, 538–541, 2018.
- 310 Berg, A. and McColl, K. A.: No projected global drylands expansion under greenhouse warming,
311 *Nat. Clim. Chang.*, 11, 331–337, <https://doi.org/10.1038/s41558-021-01007-8>, 2021.
- 312 Denissen, J. M., Teuling, A. J., Pitman, A. J., Koirala, S., Migliavacca, M., Li, W., Reichstein, M.,
313 Winkler, A. J., Zhan, C., and Orth, R.: Widespread shift from ecosystem energy to water limitation
314 with climate change, *Nature Climate Change*, 12, 677–684, 2022.
- 315 Feng, S. and Fu, Q.: Expansion of global drylands under a warming climate, *Atmospheric Chemistry
316 and Physics*, 13, 10081–10094, <https://doi.org/10.5194/acp-13-10081-2013>, 2013.
- 317 Feng, S., Gu, X., Luo, S., Liu, R., Gulakhmadov, A., Slater, L. J., Li, J., Zhang, X., and Kong, D.:
318 Greenhouse gas emissions drive global dryland expansion but not spatial patterns of change in
319 aridification, *Journal of Climate*, 35, 2901–2917, 2022.
- 320 Fensholt, R., Langanke, T., Rasmussen, K., Reenberg, A., Prince, S. D., Tucker, C., Scholes, R. J.,
321 Le, Q. B., Bondeau, A., and Eastman, R.: Greenness in semi-arid areas across the globe 1981–
322 2007—an Earth Observing Satellite based analysis of trends and drivers, *Remote sensing of
323 environment*, 121, 144–158, 2012.
- 324 Fu, B., Stafford-Smith, M., Wang, Y., Wu, B., Yu, X., Lv, N., Ojima, D. S., Lv, Y., Fu, C., Liu, Y.,
325 Niu, S., Zhang, Y., Zeng, H., Liu, Y., Liu, Y., Feng, X., Zhang, L., Wei, Y., Xu, Z., Li, F., Cui, X.,
326 Diop, S., and Chen, X.: The Global-DEP conceptual framework — research on dryland ecosystems
327 to promote sustainability, *Current Opinion in Environmental Sustainability*, 48, 17–28,
328 <https://doi.org/10.1016/j.cosust.2020.08.009>, 2021.
- 329 Grünzweig, J. M., De Boeck, H. J., Rey, A., Santos, M. J., Adam, O., Bahn, M., Belnap, J., Deckmyn,
330 G., Dekker, S. C., Flores, O., Gliksman, D., Helman, D., Hultine, K. R., Liu, L., Meron, E., Michael,
331 Y., Sheffer, E., Throop, H. L., Tzuk, O., and Yakir, D.: Dryland mechanisms could widely control
332 ecosystem functioning in a drier and warmer world, *Nat Ecol Evol*, 6, 1064–1076,
333 <https://doi.org/10.1038/s41559-022-01779-y>, 2022.
- 334 He, B., Wang, S., Guo, L., and Wu, X.: Aridity change and its correlation with greening over
335 drylands, *Agricultural and Forest Meteorology*, 278, 107663,
336 <https://doi.org/10.1016/j.agrformet.2019.107663>, 2019.
- 337 Hickler, T., Eklundh, L., Seaquist, J. W., Smith, B., Ardö, J., Olsson, L., Sykes, M. T., and Sjöström,
338 M.: Precipitation controls Sahel greening trend, *Geophysical Research Letters*, 32, 2005.



- 339 Howell, T. A. and Dusek, D. A.: Comparison of vapor-pressure-deficit calculation methods--
340 Southern High Plains, 1995.
- 341 Huang, J., Yu, H., Guan, X., Wang, G., and Guo, R.: Accelerated dryland expansion under climate
342 change, *Nature Clim Change*, 6, 166–171, <https://doi.org/10.1038/nclimate2837>, 2016.
- 343 Huang, J., Li, Y., Fu, C., Chen, F., Fu, Q., Dai, A., Shinoda, M., Ma, Z., Guo, W., Li, Z., Zhang, L.,
344 Liu, Y., Yu, H., He, Y., Xie, Y., Guan, X., Ji, M., Lin, L., Wang, S., Yan, H., and Wang, G.: Dryland
345 climate change: Recent progress and challenges, *Reviews of Geophysics*, 55, 719–778,
346 <https://doi.org/10.1002/2016RG000550>, 2017.
- 347 Huang, X., Luo, G., Ye, F., and Han, Q.: Effects of grazing on net primary productivity,
348 evapotranspiration and water use efficiency in the grasslands of Xinjiang, China, *Journal of Arid
349 Land*, 10, 588–600, 2018.
- 350 Jung, M., Reichstein, M., Ciais, P., Seneviratne, S. I., Sheffield, J., Goulden, M. L., Bonan, G.,
351 Cescatti, A., Chen, J., de Jeu, R., Dolman, A. J., Eugster, W., Gerten, D., Gianelle, D., Gobron, N.,
352 Heinke, J., Kimball, J., Law, B. E., Montagnani, L., Mu, Q., Mueller, B., Oleson, K., Papale, D.,
353 Richardson, A. D., Rouspard, O., Running, S., Tomelleri, E., Viovy, N., Weber, U., Williams, C.,
354 Wood, E., Zaehle, S., and Zhang, K.: Recent decline in the global land evapotranspiration trend due
355 to limited moisture supply, *Nature*, 467, 951–954, <https://doi.org/10.1038/nature09396>, 2010.
- 356 Jung, M., Koiraal, S., Weber, U., Ichii, K., Gans, F., Camps-Valls, G., Papale, D., Schwalm, C.,
357 Tramontana, G., and Reichstein, M.: The FLUXCOM ensemble of global land-atmosphere energy
358 fluxes, *Sci Data*, 6, 74, <https://doi.org/10.1038/s41597-019-0076-8>, 2019.
- 359 Li, C., Fu, B., Wang, S., Stringer, L. C., Wang, Y., Li, Z., Liu, Y., and Zhou, W.: Drivers and impacts
360 of changes in China’s drylands, *Nat Rev Earth Environ*, 2, 858–873, <https://doi.org/10.1038/s43017-021-00226-z>, 2021.
- 362 Lian, X., Piao, S., Chen, A., Huntingford, C., Fu, B., Li, L. Z. X., Huang, J., Sheffield, J., Berg, A.
363 M., Keenan, T. F., McVicar, T. R., Wada, Y., Wang, X., Wang, T., Yang, Y., and Roderick, M. L.:
364 Multifaceted characteristics of dryland aridity changes in a warming world, *Nat Rev Earth Environ*,
365 2, 232–250, <https://doi.org/10.1038/s43017-021-00144-0>, 2021.
- 366 Martens, B., Miralles, D. G., Lievens, H., Van Der Schalie, R., De Jeu, R. A., Fernández-Prieto, D.,
367 Beck, H. E., Dorigo, W. A., and Verhoest, N. E.: GLEAM v3: Satellite-based land evaporation and
368 root-zone soil moisture, *Geoscientific Model Development*, 10, 1903–1925, 2017.
- 369 Milly, P. C. D. and Dunne, K. A.: Potential evapotranspiration and continental drying, *Nature Clim
370 Change*, 6, 946–949, <https://doi.org/10.1038/nclimate3046>, 2016.
- 371 Mu, Q., Zhao, M., and Running, S. W.: Improvements to a MODIS global terrestrial
372 evapotranspiration algorithm, *Remote Sensing of Environment*, 115, 1781–1800,
373 <https://doi.org/10.1016/j.rse.2011.02.019>, 2011.
- 374 Pan, N., Wang, S., Liu, Y., Li, Y., Xue, F., Wei, F., Yu, H., and Fu, B.: Rapid increase of potential



- 375 evapotranspiration weakens the effect of precipitation on aridity in global drylands, *Journal of Arid*
376 *Environments*, 186, 104414, <https://doi.org/10.1016/j.jaridenv.2020.104414>, 2021.
- 377 Poulter, B., Frank, D., Ciais, P., Myneni, R. B., Andela, N., Bi, J., Broquet, G., Canadell, J. G.,
378 Chevallier, F., and Liu, Y. Y.: Contribution of semi-arid ecosystems to interannual variability of the
379 global carbon cycle, *Nature*, 509, 600–603, 2014.
- 380 Poyatos, R., Granda, V., Flo, V., Adams, M. A., Adorján, B., Aguadé, D., Aidar, M. P., Allen, S.,
381 Alvarado-Barrientos, M. S., and Anderson-Teixeira, K. J.: Global transpiration data from sap flow
382 measurements: the SAPFLUXNET database, *Earth System Science Data*, 13, 2607–2649, 2021.
- 383 Právělie, R.: Drylands extent and environmental issues. A global approach, *Earth-Science Reviews*,
384 161, 259–278, <https://doi.org/10.1016/j.earscirev.2016.08.003>, 2016.
- 385 Ramón Vallejo, V., Smanis, A., Chirino, E., Fuentes, D., Valdecantos, A., and Vilagrosa, A.:
386 Perspectives in dryland restoration: approaches for climate change adaptation, *New Forests*, 43,
387 561–579, 2012.
- 388 Reynolds, J. F., Smith, D. M. S., Lambin, E. F., Turner, B. L., Mortimore, M., Batterbury, S. P. J.,
389 Downing, T. E., Dowlatabadi, H., Fernández, R. J., Herrick, J. E., Huber-Sannwald, E., Jiang, H.,
390 Leemans, R., Lynam, T., Maestre, F. T., Ayarza, M., and Walker, B.: Global Desertification: Building
391 a Science for Dryland Development, *Science*, 316, 847–851,
392 <https://doi.org/10.1126/science.1131634>, 2007.
- 393 Roderick, M. L., Greve, P., and Farquhar, G. D.: On the assessment of aridity with changes in
394 atmospheric CO₂, *Water Resources Research*, 51, 5450–5463, 2015.
- 395 Ryu, Y., Jiang, C., Kobayashi, H., and Detto, M.: MODIS-derived global land products of shortwave
396 radiation and diffuse and total photosynthetically active radiation at 5 km resolution from 2000,
397 *Remote Sensing of Environment*, 204, 812–825, <https://doi.org/10.1016/j.rse.2017.09.021>, 2018.
- 398 Shi, H., Luo, G., Hellwich, O., Xie, M., Zhang, C., Zhang, Y., Wang, Y., Yuan, X., Ma, X., Zhang,
399 W., Kurban, A., De Maeyer, P., and Van de Voorde, T.: Evaluation of water flux predictive models
400 developed using eddy-covariance observations and machine learning: a meta-analysis, *Hydrology*
401 *and Earth System Sciences*, 26, 4603–4618, <https://doi.org/10.5194/hess-26-4603-2022>, 2022a.
- 402 Shi, H., Luo, G., Hellwich, O., Kurban, A., De Maeyer, P., and Van de Voorde, T.: Revisiting and
403 attributing the global controls on terrestrial ecosystem functions of climate and plant traits at
404 FLUXNET sites with causal networks, *Biogeosciences Discussions*, 1–22,
405 <https://doi.org/10.5194/bg-2022-191>, 2022b.
- 406 Shi, Y., Shen, Y., Kang, E., Li, D., Ding, Y., Zhang, G., and Hu, R.: Recent and future climate change
407 in northwest China, *Climatic change*, 80, 379–393, 2007.
- 408 Yang, Y., Zhang, S., McVicar, T. R., Beck, H. E., Zhang, Y., and Liu, B.: Disconnection Between
409 Trends of Atmospheric Drying and Continental Runoff, *Water Resources Research*, 54, 4700–4713,
410 <https://doi.org/10.1029/2018WR022593>, 2018.



- 411 Yao, J., Liu, H., Huang, J., Gao, Z., Wang, G., Li, D., Yu, H., and Chen, X.: Accelerated dryland
412 expansion regulates future variability in dryland gross primary production, *Nat Commun*, 11, 1665,
413 <https://doi.org/10.1038/s41467-020-15515-2>, 2020.
- 414 Yao, Y., Liu, Y., Wang, Y., and Fu, B.: Greater increases in China's dryland ecosystem vulnerability
415 in drier conditions than in wetter conditions, *Journal of Environmental Management*, 291, 112689,
416 2021.
- 417 Zeng, Y., Hao, D., Huete, A., Dechant, B., Berry, J., Chen, J. M., Joiner, J., Frankenberg, C., Bond-
418 Lamberty, B., Ryu, Y., Xiao, J., Asrar, G. R., and Chen, M.: Optical vegetation indices for
419 monitoring terrestrial ecosystems globally, *Nat Rev Earth Environ*, 1–17,
420 <https://doi.org/10.1038/s43017-022-00298-5>, 2022.
- 421 Zhang, K., Kimball, J. S., Nemani, R. R., and Running, S. W.: A continuous satellite-derived global
422 record of land surface evapotranspiration from 1983 to 2006, *Water Resources Research*, 46,
423 <https://doi.org/10.1029/2009WR008800>, 2010.
- 424 Zhao, M., A, G., Liu, Y., and Konings, A. G.: Evapotranspiration frequently increases during
425 droughts, *Nat. Clim. Chang.*, 12, 1024–1030, <https://doi.org/10.1038/s41558-022-01505-3>, 2022.
- 426 Zhao, W. L., Gentine, P., Reichstein, M., Zhang, Y., Zhou, S., Wen, Y., Lin, C., Li, X., and Qiu, G.
427 Y.: Physics-Constrained Machine Learning of Evapotranspiration, *Geophysical Research Letters*,
428 46, 14496–14507, <https://doi.org/10.1029/2019GL085291>, 2019.
- 429 Zhu, Z., Piao, S., Myneni, R. B., Huang, M., Zeng, Z., Canadell, J. G., Ciais, P., Sitch, S.,
430 Friedlingstein, P., and Arneeth, A.: Greening of the Earth and its drivers, *Nature climate change*, 6,
431 791–795, 2016.
- 432